Journal of Physics:
Conference Series

PAPER • **OPEN ACCESS**

Hydrogen, methane and one of their fuel blends combustion: CFD analysis and numerical-experimental comparisons of fixed and mobile applications

To cite this article: M Madia *et al* 2023 *J. Phys.: Conf. Ser.* **2648** 012080

Hydrogen, methane and one of their fuel blends combustion: CFD analysis and numerical-experimental comparisons of fixed and mobile applications

M Madia[1], G Cicalese[1], L Dalseno[1]

[1] R&D CFD SRL, Via Tacito 59, 41123, Modena, Italy

manuel.madia@red-cfd.it, giuseppe.cicalese@red-cfd.it, luca.dalseno@red-cfd.it

Abstract. The capabilities of Computational Fluid Dynamics (CFD) coupled with detailed chemistry simulations are examined in both steady jet diffusion flames and in an internal combustion engine case fuelled with hydrogen. Different approaches to turbulence-chemistry interaction such as the "Laminar Flame Concept" the "Eddy Dissipation Concept" and the "Turbulent Flame Speed Closure" are considered and tested. The results are compared with the experimental data available. Concerning the jet diffusion flames, the combustion processes of hydrogen, methane and one of their fuel blends are investigated on two burner geometries. Different sensitivities (i.e. mesh, turbulence model, turbulent Schmidt number, chemical mechanism) are performed. The study demonstrates that despite the burner geometry considered and the chemical composition of the fuel, the Complex Chemistry with "Eddy Dissipation Concept" is the model that better describes the behaviour of the turbulent flames. On the other hand, the "Laminar Flame Concept" sub-model is characterized by an higher fuel consumption rate, which causes an overestimation of the temperature peak. As for the in-cylinder unsteady simulations, the hydrogen combustion process is better described by the "Turbulent Flame Speed Closure" sub-model, which, unlike the other two, requires the specification of both laminar and turbulent flame speed. Despite different variations being considered, the "Laminar Flame Concept" adoption leads to an unphysically high burning rate, while the Eddy Dissipation Concept sub-model is characterized by an underestimation of the apparent heat release rate, and thus of the pressure peak inside the combustion chamber.

1. Introduction

The need of reducing CO_2 emissions is even more on top of European institutions agenda aiming to contain the dramatic effects on everyday human life related to climate change. The transportation sector is responsible for 14% of the global pollution produced worldwide and it is one of the areas where the legislation will massively impact in the next years. In Europe, a 55% reduction of emissions from new vehicles is planned for 2030 and a zero-emission scenario is the target for 2035 [1,2].

Battery electric vehicles (BEVs), charged with renewables, are only one of the possible technologies targeting the final goal, and their massive diffusion is currently slowed down by issues related to charging times, mileage and infrastructure. In this complex scenario, that includes not only the way of using but also the electric energy production and storage, green-hydrogen might emerge as an effective energy vector to lower both dependency from fossil fuels and pollutant emissions in different hard-to-abate sectors: it could be the case of methane-hydrogen mixing to reduce the CO_2 emissions in both

ceramic sector or in the case of internal combustion engines, a widespread technology adopted not only in the transportation sector. Hydrogen produced through renewables is very attractive and can help in introducing an even higher amount of discontinuous renewable energy in the current energetic mix and, thanks to its flexibility, it can be used as a fuel in ready-made technologies reducing the time needed for the energetic transition and furthermore can help the energetic transition of sectors in which the electrification is not a viable option [3].
In the current work the CFD modelling of hydrogen combustion in two very different applications such as burners and internal combustion engines is deepened with the final aim to develop reliable methodologies for the numerical study of this promising fuel. Considering the very simple hydrogen oxidation pathway, complex chemistry can be solved in the CFD code without incurring in unaffordable CPU costs but, in some applications such as ICEs, the interaction between turbulence and chemistry must be accounted for. Different CFD approaches are tested and validated on experimental data on both engine cases and burners pointing out as, despite the same simple fuel is used, a different modelling strategy is needed for the simulation of different applications.

1.1. CFD Modelling

The wide flammability range, flame speed and knock resistance allow the use of sole hydrogen as fuel in spark ignition (SI) engines. CFD simulation of cold flow, mixing and combustion in SI engines is widespread in both scientific and industrial community and can be very useful in the evaluation of the performance of alternative fuels [4, 5] when a set of reliable and validated sub-models is purposely developed [6-11]. Thanks to the reduced computational cost Reynolds Averaged Navier-Stokes (RANS) is the widely used approach for the prediction of normal and abnormal combustion despite more CPU demanding approaches such as LES (Large Eddy Simulation) can be successfully applied to account for cyclic variation of combustion due to turbulent flows [12-16]. Turbulent combustion in RANS of standard and unconventional fuels can be effectively modelled integrating fuel specific chemical characteristics, such as laminar flame speed, ignition delay times and soot tendency without solving online chemistry as demonstrated in [17-21], saving CPU time and preserving accuracy. Despite this, the direct integration of chemical kinetics in the CFD framework is becoming even more attractive thanks to the increase of computing power, especially for the simulation of combustion of fuels which oxidation pathway involves a low number of species and reactions such as hydrogen. In the current work these approaches are explored and validated in two very different applications such as burners and ICEs.

RANS coupled with detailed chemistry combustion model is firstly analysed on three jet diffusion flames whose experimental database are available in literature. Secondly, combustion analyses are carried out on a hydrogen fuelled ICE, whose in-cylinder pressure profile is available for numerical validation.

The combustion model considered is based on Complex Chemistry. The detailed chemistry information about species, reactions, thermodynamic and transport properties are specified through Chemkin format files [22, 23]. For a given species imported, the model solves an additional transport equation [Eq1]

$$\frac{\partial(\rho Y_i)}{\partial t} + \frac{\partial\left(\rho u_j Y_i\right)}{\partial x_j} = \frac{\partial}{\partial x_j}\left(\rho D_{tot}\frac{\partial(Y_i)}{\partial x_j}\right) + \dot{\omega}_i \tag{1}$$

Where Y_i is the mass fraction of the i-th species, D_{tot} is the total diffusivity, which includes the effects of turbulence as it will be explained later, and $\dot{\omega}_\iota$ which is the source/sink term. In particular, the latter is calculated as reported in Eq.2 and Eq.3

$$\dot{\omega}_\iota = \rho f\left(\frac{Y_i^* - Y_i}{\tau}\right) \tag{2}$$

$$Y_i^* = Y_i + \int_0^\tau r_k \, dt \tag{3}$$

Where τ is specified for unsteady simulations, while is defined as the resident time in a cell for steady-state simulations, Y_i^* is the mass fraction at the end of the integration, r_k is the reaction rate of the k-th reaction of the mechanism, which depends on the local chemical composition, temperature and pressure. The term f is the reaction rate multiplier, and it will be described later. As for the total diffusivity, it is calculated as in Eq.4

$$D_{tot} = D_m + D_{turb} \tag{4}$$

Where D_m is the laminar diffusivity, which can be either derived from the definitions of Schmidt and Prandtl number or can be the value imported with the transport file of the Chemkin format, while the D_{turb} term is the turbulent diffusivity and is calculated with Eq.5

$$D_{turb} = \frac{\mu_t}{\rho \, Sc_t} \tag{5}$$

Where μ_t is the turbulent viscosity and Sc_t is the turbulent Schmidt number, which is a user-defined parameter.

With the Complex Chemistry model, it is possible to choose, within STAR-CCM+ software used, different turbulence-chemistry interaction sub-models, such as the "Laminar Flame Concept" (CC-LFC), the "Eddy Dissipation Concept" (CC-EDC) and the "Turbulent Flame Speed Closure" (CC-TFC). With the CC-LFC model, f and τ of equations (2) and (3) are defined ad in Eq.6 and Eq.7

$$f = 1 \tag{6}$$

$$\tau = \tau_{res} \tag{7}$$

The CC-EDC model is based on the work of Magnussen [24, 25], in which is explained that the combustion processes take place when reactants are mixed at a molecular scale (Kolmogorov length scale) at high temperature. The reaction zone is then strongly dependent on the structure of the turbulent flow, and in particular on the local values of turbulent kinetic energy k and its dissipation ε. This dependence is considered on the definition of f and τ in the equations 8 and 9.

$$f = \left(\left[C_l \left(\frac{\nu \, \tau_{turb}}{L^2} \right)^{0.25} \right]^{-3} - 1 \right)^{-1} \tag{8}$$

$$\tau_{turb} = C_\tau \left(\frac{\nu}{\varepsilon} \right)^{1/2} \tag{9}$$

Where C_l and C_τ are model parameters, ν is the kinematic viscosity, ε the turbulent dissipation rate and L is the turbulent length scale. As it will be seen, with these definitions of the reaction rate multiplier and timescale, the reaction rate of the CC-EDC is generally lower than CC-LFC one.

As for the Turbulent Flame Speed Closure, this model requires the definition of both laminar and turbulent flame speed: it identifies the position of the flame front and propagates it at the TFS specified,

so it suitable for premixed and partially premixed combustion simulations. The CC-TFC model behaviour will be examined on the hydrogen combustion in the internal combustion engine on which, more details can be found in [26]. The laminar flame speed correlation used is the one proposed by Verhelst et al. [27], while the Peters correlation is used for the turbulent flame speed. With CC-TFC is also possible to activate the Relax to Chemical Equilibrium (CC-RTCE) option, which reduces the computational expanse of the simulation since all the reaction are frozen in the unburnt zone, while the chemical composition rapidly relaxes to the local equilibrium.

2. Jet Flames

As mentioned in the first section, the Complex Chemistry combustion model is initially tested on three diffusion jet flame, whose structure and characteristics can be found in literature [28-32]. In particular, the first one (Sandia Flame D) is a methane piloted jet flame, used for models benchmarking on a more conventional hydrocarbon, while the other two (DLR_A and H3 Flames) consider respectively a blending between methane and hydrogen and a mixture of hydrogen and molecular nitrogen. The main difference between a piloted burner and a simple one is the fact that in the former the central fuel jet is placed in an annulus of premixed flames. The heat from the pilot stabilizes the main combustion to the burner, so that the fuel velocity of this burner is generally higher compared to the simple one.

Numerical analyses are carried out with steady-state RANS simulations on the commercial code STAR-CCM+ v16.06. For each case, after a brief description of the geometry of the problem and of the boundary conditions, results with the different models/approaches will be reported in terms of temperature and major chemical species trends across the domain.

2.1. Sandia Piloted Jet Flame D

The Sandia piloted burner geometry consists of the main jet fuel diameter of 7.2 mm, the annulus of combustion products width of 5.25 mm, all surrounded by an unbounded standard air environment. Given the relatively simple geometry, a two-dimensional axisymmetric domain is considered, as it can be seen in figure (1a): there are three velocity inlet boundaries for the main jet, the pilot, and the co-flow, two pressure outlets (outer and outlet) and the burner axis. As for the inlet boundary conditions, even though an experimental profile for velocity and turbulence intensity can be found in literature [33], the results presented in this paper were obtained with constant values for both. In particular, the case identified by the letter D was considered and the velocity inlet values for each boundary are specified in Table1, while the turbulence intensity values are 0.075 for the main inlet, 0.1 for the pilot and 0.01 for the co-flow, with a turbulent length scale equal to the 10% of the geometric diameter. The reason for this simplification is that the overall behavior of the burner does not significantly change with pointwise values, while the computational cost of the simulation slightly increases.

In figure (1a) is also possible to visualize the mesh used for this case. It is a 5000 cells domain, with a lower-sized cells (0.5 mm) near the axis and the inlet boundaries. A mesh sensitivity was carried out, with different refinements which include a broader area near the reaction zone, as shown in figure (1b). For the sake of brevity, the results of these cases will not be included in this paper since a macroscopic difference with respect to the standard mesh could not be seen.

Regarding the chemical composition, the main jet fuel is an ambient-temperature rich mixture of methane ($\Phi = 3.18$), the pilot inlet is characterized by a lean composition ($\Phi = 0.77$) of methane combustion products at 1900 K, while the co-flow stream is a standard air boundary at 293 K. This simulation does not need an ignitor because of the presence of pilot hot burnt gases, unlike the two simple burner simulations that will be described later.

Concerning the experimental data, Raman/Rayleigh/LIF measurements of temperature and different chemical species at different location of the domain were obtained [34]. In this paper, Favre-averaged axial profiles of temperature and methane mass fraction are used for numerical-experimental comparisons. The spatial location is normalized by the main jet diameter nozzle (d_{main}). As for the simulation setup, the turbulence model considered is the *Realizable* $k-\varepsilon$ model with the *Two-Layer All-*y^+ wall treatment. A 30-species skeletal mechanism based on the GRI-3.0 [35] is here adopted.

Table 1. Velocity boundary conditions for six methane flames.

Flame	u_{main} (m/s)	u_{pilot} (m/s)	u_{coflow} (m/s)
A	2.44	-	0.9
B	18.2	6.8	0.9
C	29.7	6.8	0.9
D	49.6	11.4	0.9
E	74.4	17.1	0.9
F	99.2	22.8	0.9

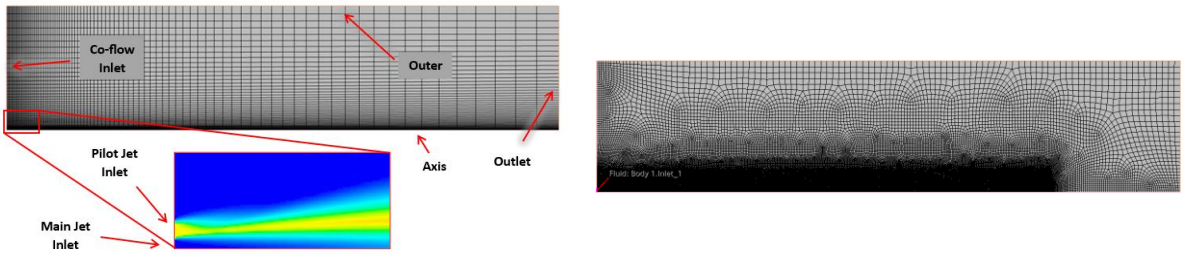

(a) (b)

Figure 1. Mesh discretization and boundary visualization for Sandia Flame D simulation (a), mesh refinement considered for the same case (b)

2.1.1. Results and discussion. The CC-LFC and CC-EDC performance are here presented and compared with the experimental data available in literature. In particular, the axial temperature trend and the axial fuel mass fraction trend are considered. In this way is possible to analyse the burn rate obtained with the two models with respect to experimental data.

As shown in the two graphs in figure (2), with the CC-LFC model is possible to see an higher fuel consumption rate with respect to the experimental trend, with the axial CH_4 mass fraction that reaches the null value at $x/d_{main} = 35$, approximately 100 mm before the experimental profile. This behavior results in an overestimation of the axial temperature in the range $10 < x/d_{main} < 50$, with a peak temperature of $2160\,K$ at $x/d_{main} = 40$, against a peak of $1920\,K$ at $x/d_{main} = 43$ of the experimental profile. On the other hand, the different formulation of the source term in the species transport equation of the Eddy Dissipation Concept sub-model results in a slower burn rate with respect to CC-LFC, with $T_{Peak} = 2030\,K$ and $x/d_{main}(T_{peak}) = 40$, and an axial temperature profile which is closer to the experimental one.

With the CC-EDC model a turbulent Schmidt number sensitivity is performed, as this is an important model constant. As seen in the section 1, by changing this parameter is possible to modify the species turbulent diffusivity, and thus the flame position. It is important to note that the turbulent Prandtl number is also modified, and it is set to the same value. The graph in figure (3) shows the axial temperature profile for four different values of turbulent Schmidt number. Standard setup, represented by the yellow trend, considers $Sc_t = 0.9$. It can be noticed that by increasing Sc_t, and thus by reducing the total diffusivity, the peak temperature is reached at higher x/d_{main}. With $Sc_t = 1.2$, the axial temperature profile in the first half of the domain is closer to the experimental one compared to the standard setup, while from $x/d_{main} = 40$ an overestimation of over $200\,K$ can be noted. Nevertheless, all the simulations present the same value of temperature peak. Thus, since the overall behavior of the burner is not improved, the next simulations will consider the standard value of Sc_t and Pr_t.

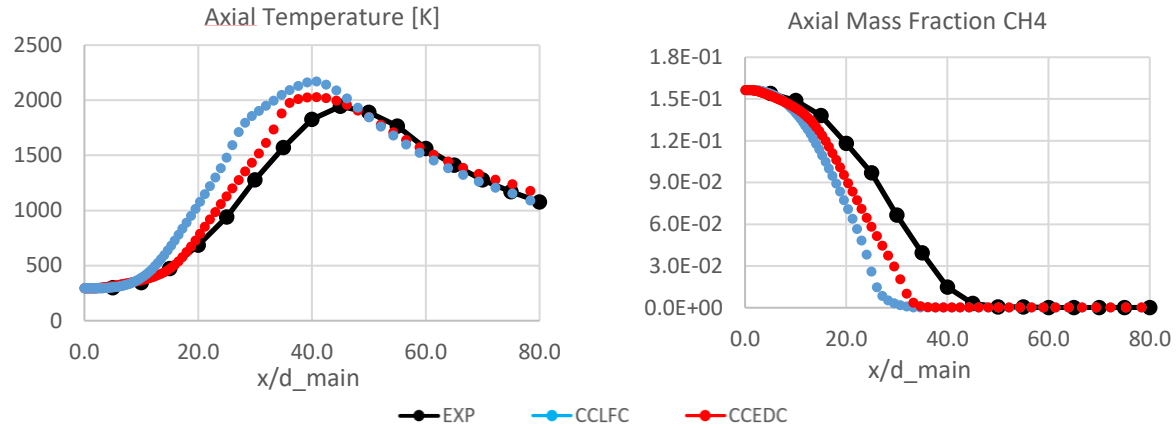

Figure 2. Axial temperature and methane mass fraction profiles.

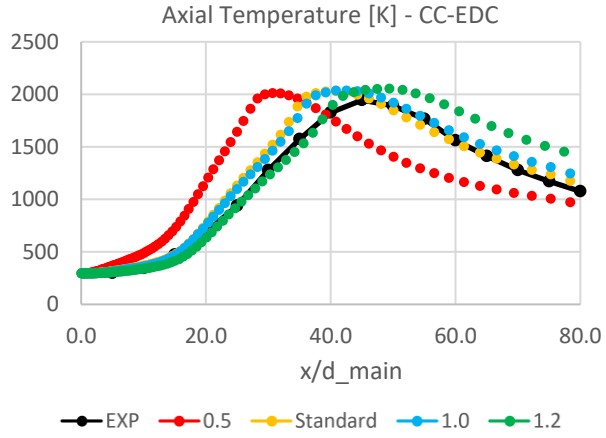

Figure 3. Axial temperature profiles for CC-EDC model with four different values of the turbulent Schmidt number.

2.2. DLR_A Simple Jet Flame

The simple jet burner geometry consists of the main jet fuel diameter of 8.0 mm, surrounded by an unbounded standard air environment. As in the previous case, a two-dimensional axisymmetric geometry is considered, with two velocity inlet boundaries, the main jet inlet and the co-flow inlet, two pressure outlet boundaries, renamed outer and outlet, and the burner axis (figure (4a)). In order to start the combustion process, an ignitor is added to the domain at the interface between the fuel and the oxidizer flow, whose temperature is set at 1800 K.

The boundary conditions specified are available on the TNF Workshop data archives website [36]. In this section the *DLR_A* flame is examined: the fuel chemical composition is a mixture of methane, hydrogen and nitrogen, respectively 22.1%-33.2%-44.7% by volume, while the co-flow inlet composition, as in the previous case, is a standard air inlet. Concerning the inlet velocities and turbulence specifications, a constant value for each inlet is considered: the main jet inlet velocity is set to 42.2 m/s, with a turbulence intensity of 0.1 and a turbulent length scale equal to the 10% of the geometric diameter; as for the co-flow inlet, the velocity is set to 0.3 m/s, with a turbulence intensity of 0.01 and a turbulent length scale equal to 2.0 mm. Both fuel and oxidizer streams temperature are set as 293 K.

In figure (4b) is represented the 60000 cells mesh used for these simulations, with a minimum size of 0.5 mm near the inlet boundaries and burner axis and a maximum cell size of 5.0 mm in the outer region. The domain axial extension is 0.8 m, while the radial one is 0.13 m. The chemical mechanism used is the GRI-3.0, which is a 53-species and 325-reactions methane oxidation mechanism that include the hydrogen chemistry and NO formation. As for the turbulence model, the *Realizable* $k-\varepsilon$ model with the *Two-Layer All-*y^+ wall treatment is considered.

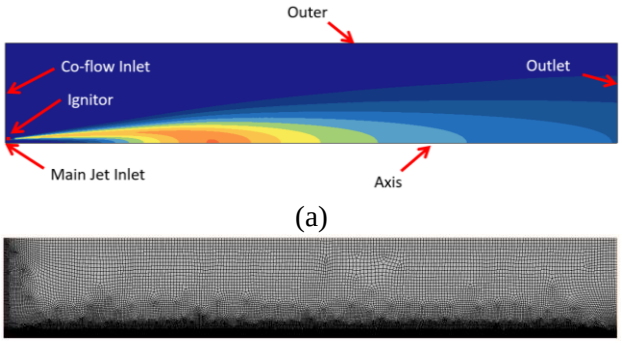

Figure 4. Boundary specification (a) and mesh visualization (b) for the simple jet diffusion flames simulations.

2.2.1. Results and discussion. The CC-LFC and CC-EDC performance are examined on the methane/hydrogen combustion processes on the DLR_A simple jet burner geometry. The results are presented in terms of axial profiles of temperature, methane mass fraction and hydrogen mass fraction. While in the Sandia Piloted Flame D the difference between the two models was evident, with this flame the two models are characterized by comparable fuel consumption rates. With CC-LFC the CH_4 mass fraction decreases slightly faster than CC-EDC, while the H_2 mass fraction profiles are almost overlapped. In terms of temperature, the CC-EDC model is the one that better describes the combustion processes, with a peak temperature of $2028\ K$ at $x/d_{main} = 63$, while with the Laminar Flame Concept $T_{peak} = 2088\ K$ at $x/d_{main} = 61$, against the experimental data of $T_{peak} = 1850\ K$ at $x/d_{main} = 60$. After the temperature peak, both models show an overestimation of $200 \div 300\ K$ up to the outlet boundary.

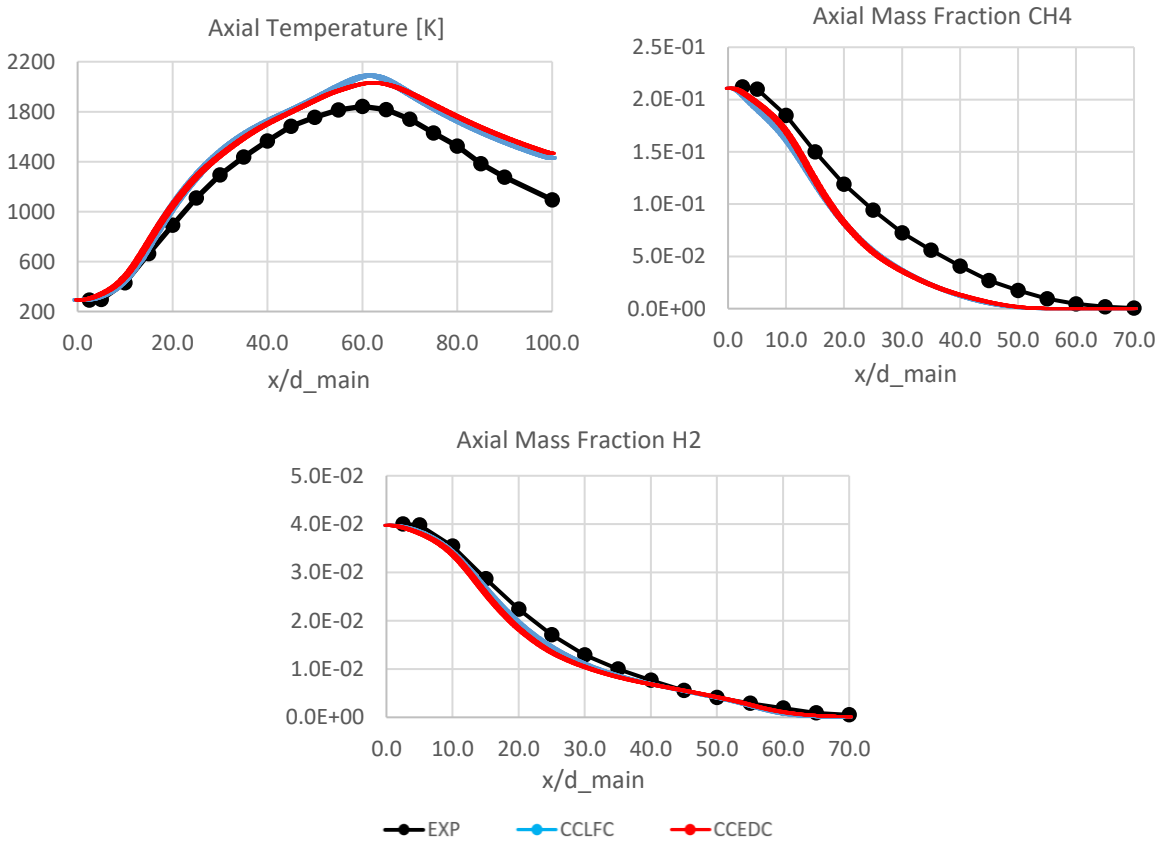

Figure 5. Axial temperature, methane and hydrogen mass fractions profiles.

2.3. H3 Simple Jet Flame

The last case consists of an hydrogen simple jet flame that uses the same burner geometry seen in the *DLR_A* simple flame, and for this reason, the same 60000 cells domain is considered. Concerning the main jet chemical composition, a mixture of 50%-50% by volume of hydrogen and nitrogen is set as boundary condition for the main jet, while a standard air composition is specified at the co-flow inlet. Moreover, the main jet is characterized by a 34.4 m/s inlet velocity, and the co-flow a value of 0.3 m/s is imposed. The turbulence specification is the same as *DLR_A* setup.

As for the simulation setup, the 10-species and 21-reactions hydrogen oxidation mechanism provided by the Lawrence Livermore National Laboratory [37] is imported in Chemkin format. Concerning the turbulence model, as in the previous cases, the *Realizable* $k-\varepsilon$ *model* with the *Two-Layer All-*y^+ wall treatment is considered.

2.3.1. Results and discussion. The CC-LFC and CC-EDC resulting axial trends for temperature, H_2 and H_2O mass fractions are compared to the experimental database available on the DLR Institute website [38]. As already seen, the spatial position is normalized by the main jet diameter, which for this burner is equal to 8.0 mm. Analogously to the methane/hydrogen simple flame, Laminar Flame Concept and Eddy Dissipation Concept show comparable burn rates, since the two H_2 mass fraction profiles are almost overlapped. With the same turbulence field, both models show a fuel consumption which is coherent with the experimental data available. The only notable difference can be seen in the temperature field, and likewise in the H_2O mass fraction graph, in which the CC-LFC presents an higher overestimation of the peak: while the experimental value is $T_{peak} = 1750\ K$ and the CC-EDC one is $T_{peak} = 1860\ K$, the resulting value from the CC-LFC simulation is $T_{peak} = 1950\ K$. Despite these differences, the three profiles show a similar peak temperature location that lays near $x/d_{main} = 35$.

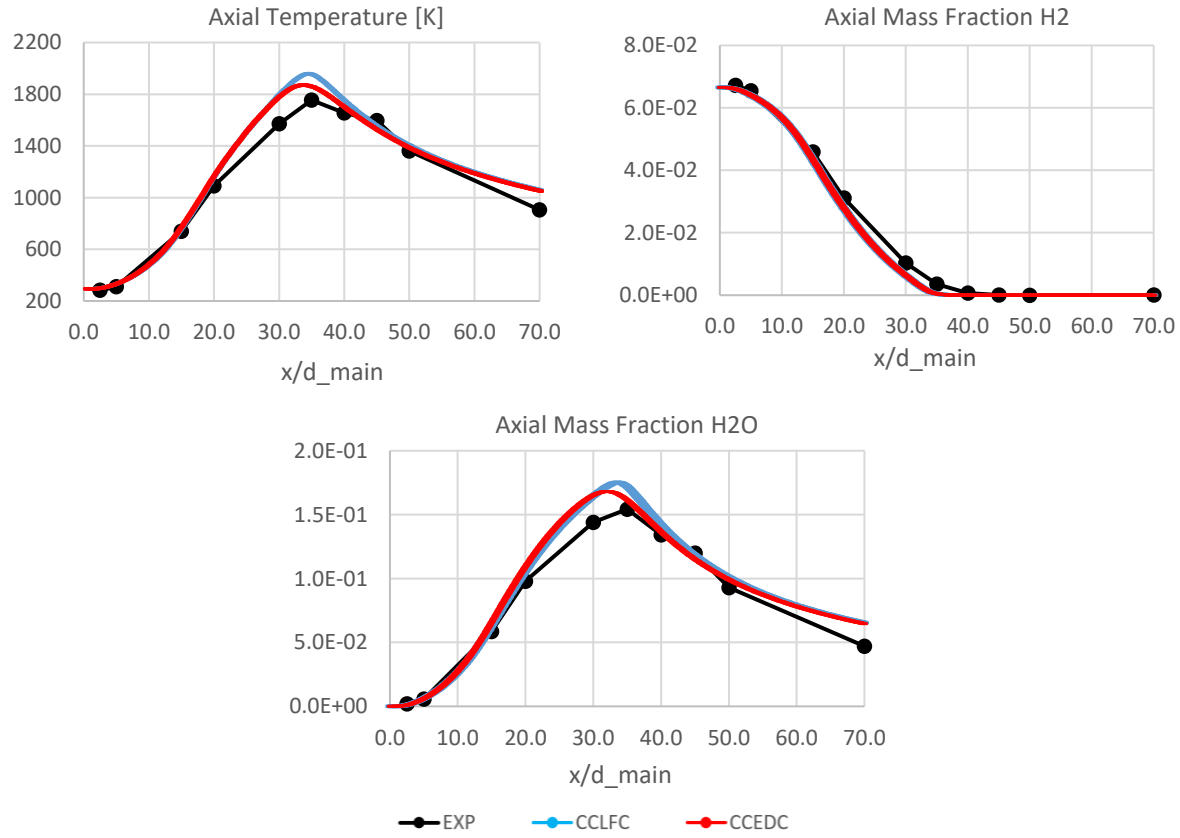

Figure 6. Axial temperature, hydrogen and vapor water mass fractions profiles.

3. Internal Combustion Engine

After the validation of the combustion models on three jet diffusion flame reported in the previous section, the Complex Chemistry model behaviour is examined on the hydrogen combustion in engine-like conditions.

The analysed engine is a naturally aspirated, single cylinder whose computer aided design (CAD) is reported in figure (7). Originally, it was a CI engine with a 19:1 compression ratio. It was properly modified as described in [39] and [40] in order to allow the hydrogen combustion as in a SI engine. The main characteristics of the analysed version are listed in table (2).

Table 2. Main characteristics of the investigated engine.

Displaced Volume [cm^3]	505
Bore [mm]	85
Stroke [mm]	87
Compression Ratio	10:1

Experimental in-cylinder pressure trace was recorded for 100 cycles for twelve different load condition; in this paper the 2500 rpm, part load, with a global lean mixture ($\Phi = 0.6$) is considered.

Since the work of this paper is focused on the assessment of detailed chemistry combustion model, the simulations will refer only on the range between 700 degCA, 12.5 degCA before the spark ignition, and 810 degCA, i.e. half of the expansion stroke.

The combustion analyses will be carried out in two steps: in section 3.1 the models will be tested on a simplified, constant-volume combustion chamber obtained from the original CAD shown in figure (7), while in section 3.2 the simulations will be performed considering a more realistic moving mesh configuration.

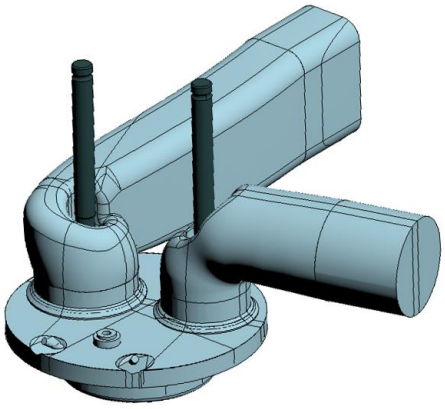

Figure 7. Investigated engine geometry.

3.1. Constant-volume combustion chamber

The geometry considered for the cases that will be shown in this section is represented in figure (8). From the standard geometry in figure (7), only the combustion chamber at 712 degCA (spark time), the spark plug and the injectors are considered. Furthermore, in order to reduce the computational cost and thus the simulation time, and given the symmetric domain, only half of the geometry is studied.

The mesh used for this case is represented in figure (8): a trimmed mesher with a 1.0 mm sized cell was chosen, with a single near wall prism layer with a thickness of 0.35 mm. It is also visible the 0.5 mm refinement performed on a 5.0 mm radius sphere whose origin coincides with the spark plug one.

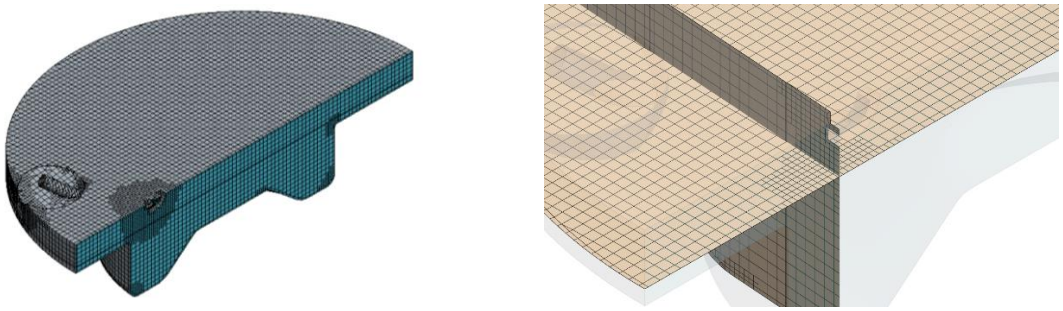

(a) (b)

Figure 8. Standard mesh discretization for the constant volume simulations (a), with a close-up view of two sections near the spark plug (b).

3.1.1. Simulation setup. The hydrogen combustion development is analysed with unsteady-RANS simulations. The initial conditions considered for pressure, temperature, velocity, chemical composition, turbulent kinetic energy and its dissipation are the result of a full cycle simulation including H_2 direct injection whose details are reported in [26]. As for the boundary conditions, for model assessment wall heat transfer is neglected setting all the walls as adiabatic walls. In order to ignite the mixture, a 1.0 mm diameter sphere is initialized in the domain with a temperature of $1500\,K$ promoting the onset of chemical reactions. The standard case considers a constant time-step of $1.0 \cdot 10^{-6}$ s. Concerning the turbulence modelling, as in the jet flame cases, the *Realizable* $k-\varepsilon$ with the *Two-Layer All-*y^+ wall treatment model is used.

As for the flame propagation, CC-LFC and CC-EDC are here compared to the CC-TFC model, in which both laminar flame speed and turbulent flame speed are respectively calculated by Verhelst and Peters correlation. The result obtained with this last model will be considered as a reference due to the suitability of this approach for the prediction of burn rate in highly turbulent flows experienced in ICEs.

Moreover, the CC-TFC with Relax to Chemical Equilibrium is also examined in order to isolate the effect of complex chemistry on the results. The chemical mechanism adopted is the same used in section 2.3, the 10-species 21-reactions mechanism provided by Lawrence Livermore National Laboratory.

3.1.2. Results and discussion. The results will be given in terms of mass-averaged pressure inside the chamber and Apparent Heat Release Rate. As it can be seen in graphs in figure (9), CC-TFC and CC-RTCE present a comparable behaviour, and it can be seen also with the combustion indicators (MFB1, MFB5, etc.) and duration (CombDur0-1, CombDur0-5, etc.), where the only noteworthy difference is the CombDur50-90 values, with the CC-TFC duration equal to 7.26 degCA and the CC-RTCE one equal to 8.50 degCA. A shorter late combustion duration is promoted by the activation of complex chemistry in the end-gas when using CC-TFC.

As for LFC and EDC in engine-like conditions, the discrepancy between these two sub-models, with respect to the steady-state jet diffusion flames simulations, increases. CC-LFC is characterized by an unphysically fast hydrogen burn rate, as visible also from the Apparent Heat Release Rate profile. This behaviour is also evident with the combustion indicators and durations values: CC-TFC MFB90 is equal to 17.25 degCA, the Laminar Flame Concept one is almost half of it, with a value of 9.44 degCA, and with the combustion duration from 50% to 90% of the mass fraction burnt equal to 3.59 degCA. On the other hand, the reduction of burn rate expected from CC-EDC leads to an underestimation of the hydrogen burn rate with respect to the CC-TFC model. The AHHR profile shows that the combustion process take place during the overall considered physical time, with a 90% of mass fraction burnt that is reached after 44 degCA, and the maximum pressure value is reached only at the end of the simulation.

Different sensitivities were performed when using the CC-LFC model. Since the molecular diffusivity of the standard setup is evaluated from the Schmidt number, the kinetic theory method, which calculates the molecular diffusivity from the transport file of the chemical mechanism, was also tested, but no remarkable differences in the model behavior can be noticed. Hence, the unity Lewis number can

be adopted even with turbulent combustion of hydrogen, which is characterized, due to its high mass diffusivity, by a Lewis number equal to 0.3. Nevertheless, the kinetic theory method should be used when the turbulence effects decrease, and thus the effect D_{turb} on the total diffusivity value, in order to account for the hydrogen flame instabilities. As for the chemical mechanism, the 21-species and 62-reactions H_2/CO Chemkin file provided by CRECK Modeling Group [41] was also considered, but the only noteworthy difference with this setup is an increasing solving time due to the higher number of species and reactions.

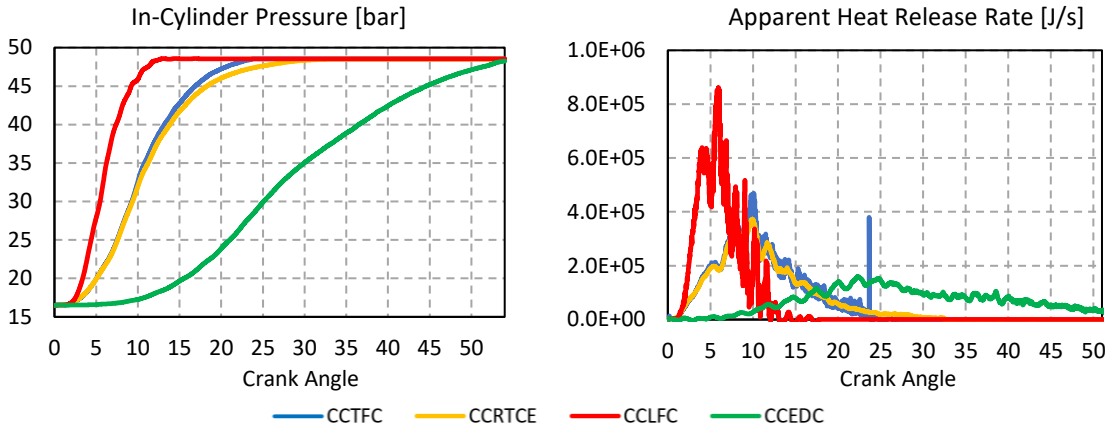

Figure 9. Pressure and Apparent Heat Release Rate profiles for the constant-volume simulations.

Table 3. Combustion indicators and durations for the constant volume simulations. Results are reported in Crank Angle degrees considering a revving speed of 2500 rpm.

	CCTFC	CCRTCE	CCLFC	CCEDC
Start of Combustion [degCA]	0.15	0.15	0.15	0.15
MFB 1 [degCA]	2.17	2.11	2.01	7.77
MFB 5 [degCA]	3.76	3.72	2.79	12.14
MFB 10 [degCA]	4.86	4.88	3.30	15.03
MFB 50 [degCA]	9.99	10.17	5.85	27.15
MFB 90 [degCA]	17.25	18.67	9.44	44.75
CombDur 0-1 [degCA]	2.02	1.96	1.86	7.62
CombDur 0-5 [degCA]	3.61	3.57	2.64	11.99
CombDur 10-50 [degCA]	5.13	5.30	2.55	12.12
CombDur 50-90 [degCA]	7.26	8.50	3.59	17.60

3.2. Moving piston configuration

The geometry considered for the moving mesh cases is represented in figure (11). Unlike the constant volume setup, the entire domain is here considered. As in the section 3.1, in order to compare the models, results will be presented in terms of mass-averaged pressure inside the combustion chamber and Apparent Heat Release Rate. As for experimental trends, the 100-cycle ensemble averaged pressure profile is used for model validation.

3.2.1. Simulation setup. The chemical mechanism imported is the one developed by the Lawrence Livermore National Laboratory, already described in the previous sections. As for the mesh, the discretization is visible in figure (11): a trimmer mesher is considered, with a 1.0 mm cell size for the combustion chamber and a 0.5 mm sphere-shaped volume refinement whose centre corresponds to the

spark location and with a radius of 10 mm. Concerning the ignition, the imposed stretch spark ignition model (ISSIM) is activated and the same parameters for all the models are set. The turbulence is modelled with the RNG $k-\varepsilon$ model, and the Gru-MO Unimore wall treatment formulation [42-44] is considered to calculate heat fluxes. As for the time discretization, a stepped time step is considered: in the range from 710 degCA to 725 degCA, $\Delta t = 0.025$ degCA, then $\Delta t = 0.05$ degCA until 752 degCA, and $\Delta t = 0.1$ degCA up to the end of the simulation. Constant temperature boundary conditions are specified, while the pressure, temperature, velocity, mixture composition and turbulence initial conditions are the same used in the constant-volume chamber.

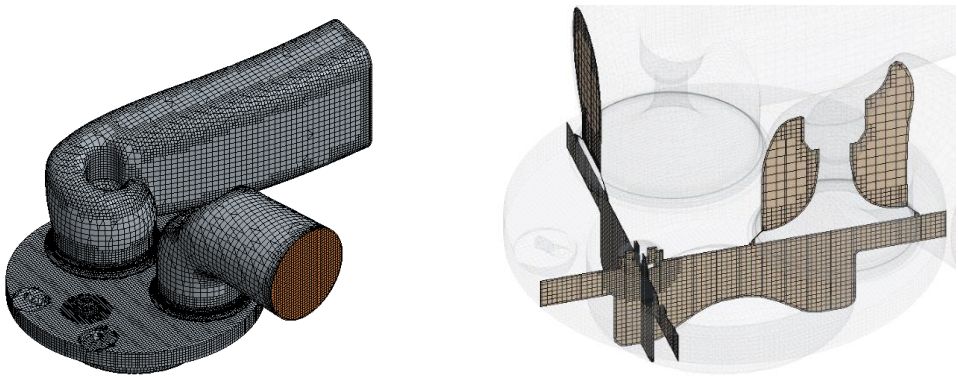

(a) (b)

Figure 10 . Mesh discretization for the in-cylinder simulations (a), with a view of two sections near the spark plug (b).

3.2.2. Results and discussion. CC-TFC is the model that better describes the combustion development for this case. In fact, both pressure traces, with and without Relax to Chemical Equilibrium option, are in good agreement with the experimental profile, with the CC-RTCE model that presents a slightly closer values with respect to CC-TFC and, due to the simplified approach, lower solving time. As in the constant-volume cases, the similar results obtained with these two approaches suggest that end-gas chemistry activated with CC-TFC has not a major influence on the combustion process in this case.

As for CC-EDC, as seen in the model assessment performed on the constant-volume geometry, the hydrogen consumption rate is too low, as the Apparent Heat Release Rate profile shows, causing an underestimation of the peak pressure value of 5.0 bar. Nevertheless, the simulation results are in good agreement with the experimental profile up to 725 degCA, since MFB1, MFB5 and MFB10 indicators are comparable with the experimental values. This behaviour suggests that, unlike the constant-volume cases, with a calibration of the model parameters, such as C_l and C_τ, the combustion development can be further improved.

On the contrary, CC-LFC combustion behaviour is strongly unphysical, as the 50% of mass fraction burnt is reached 0.88 degCA before TDC, while the experimental value is 16.50 degCA after TDC. This results in a strong overestimation of the pressure inside the chamber, with a peak above 65 bar reached near the TDC, while the experimental maximum value is 37 bar at 740 degCA. Since the Laminar Flame Concept model only considers the turbulence effect through an increased molecular diffusivity, in order to capture smaller turbulent-scale structures, a mesh refinement is performed, with a 0.5 mm cell size for the combustion chamber and a 0.2 mm refinement for the sphere-shaped volume centred in the spark location. With an increased number of cells and thus the computational cost, despite the combustion development remains unphysical, a slight lower flame speed propagation with respect to the standard CC-LFC setup is visible, which results in 1.0 bar lower pressure peak, reached almost 4.0 degCA later. This behaviour indicates that it is possible to obtain a lower fuel consumption rate by performing a strong mesh refinement, and it can be useful when the fuel-dependent laminar flame speed correlation is not available and thus the CC-TFC model cannot be used.

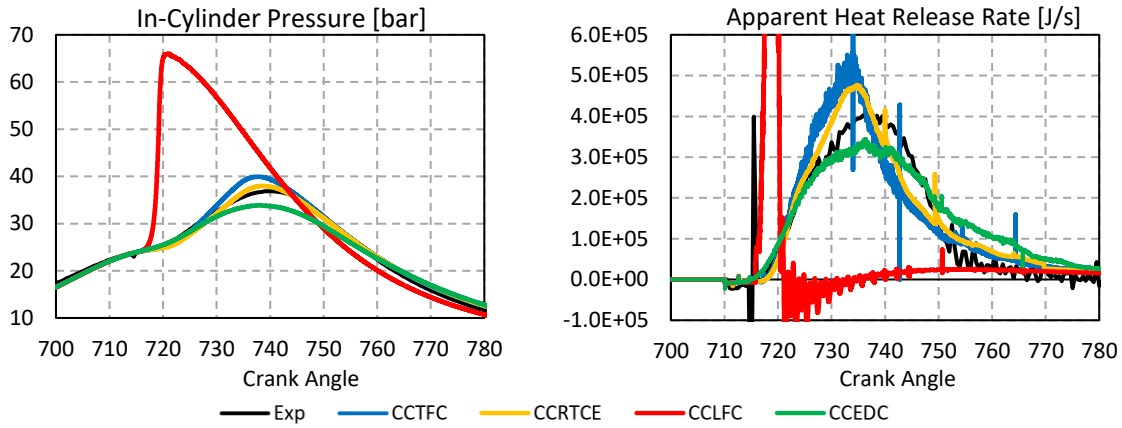

Figure 11. Pressure and Apparent Heat Release Rate profiles comparison.

Table 4. Combustion indicators for the In-Cylinder simulations

	EXP	CCTFC	CCRTCE	CCLFC	CCEDC
Start of Combustion [CA]	712.5	712.5	712.5	712.5	712.5
MFB 1 [CA aTDC]	0.50	1.23	1.48	-3.02	-0.29
MFB 5 [CA aTDC]	3.00	3.69	4.03	-2.28	3.15
MFB 10 [CA aTDC]	5.50	5.70	6.18	-1.87	5.76
MFB 50 [CA aTDC]	16.50	15.59	16.92	-0.88	20.20

4. Conclusions

The complex chemistry combustion model and three turbulence-chemistry interaction sub-models are tested on different turbulent jet diffusion flames and on a direct injection spark ignition hydrogen fuelled internal combustion engine. The results suggest the following:

- if the fuel-dependent laminar and turbulent flame speed correlations are available, CC-TFC is the most suitable model for premixed and partially premixed flame fronts, since it propagates the reaction zone at the user-imposed turbulent flame speed. If pollutant emissions and abnormal combustion phenomena are not relevant, the Relax to Chemical Equilibrium option can be activated in order to reduce the computational expanse of the simulation but keeping a good agreement with the experimental profiles.
- CC-EDC is the model that, thanks to its reaction rate multiplier f and time-scale τ formulations that include, unlike the CC-LFC model, the effect of turbulence on the flame structure, better describes the combustion development of diffusion flames in ambient-like conditions despite the fuel chemical composition. As a matter of fact, both methane and hydrogen combustion processes are in good agreement with the experimental profiles. In engine-like condition, the Eddy Dissipation Concept model tends to slightly underestimate the hydrogen burn rate, which results in a lower pressure peak inside the combustion chamber. Nevertheless, the combustion development is in good agreement with the experimental data before MFB50 is reached, which suggests that a model calibration can further improve its behavior.
- CC-LFC model tends to slightly overestimate the fuel consumption rate with respect to the CC-EDC model in hydrogen and methane jet diffusion flames. The difference between the models increases in engine-like conditions, with Laminar Flame Concept that overestimates hydrogen consumption in both constant-volume chamber and moving piston configuration, which makes it not ideal for the simulation of premixed and partially premixed hydrogen flame fronts.

Nevertheless, by performing a mesh refinement, and thus capturing an higher amount of turbulent structures, a decreasing fuel consumption rate is visible, which suggests that the implementation of a strong local refinement in correspondence of the reaction zone can lead to a more physical combustion development.

References

[1] Kalghatgi G T 2015 Developments in internal combustion engines and implications for combustion science and future transport fuels *Proceedings of the Combustion Institute* **35** 101-115. doi: 10.1016/j.proci.2014.10.002

[2] Eisele K 2021 Fit for 55 package: Recasting the Energy Efficiency Directive, Initial Appraisal of a European Commission Impact Assessment EPRS, European Parliament https://www.europarl.europa.eu/RegData/etudes/BRIE/2021/699462/EPRS_BRI(2021)699462_EN.pdf

[3] Athanasopoulou L, Bikas H and Stavropoulos P 2018 Comparative Well-to-Wheel Emissions Assessment of Internal Combustion Engine and Battery Electric Vehicles *Procedia CIRP* **78** 25-30. https://doi.org/10.1016/j.procir.2018.08.169

[4] Teodosio L, Berni F, Lanotte A and Malfi E 2022 1D/3D simulation procedure to investigate the potential of a lean burn hydrogen fuelled engine, *Journal of Physics: Conference Series*, https://dx.doi.org/10.1088/1742-6596/2385/1/012085

[5] Bozza F, Berni F, Cicci F, d'Adamo A et al. 2021 Potentials of the Oversizing and H2-Supported Lean Combustion of a VVA SI Gasoline Engine Towards Efficiency Improvement *SAE Technical Paper* 2021-24-0007. https://doi.org/10.4271/2021-24-0007

[6] Breda S, d'Adamo A, Fontanesi S, D'Orrico F et al. 2017 Numerical Simulation of Gasoline and n-Butanol Combustion in an Optically Accessible Research Engine *SAE Int. J. Fuels Lubr.* **10**(1):32-55, 2017. https://doi.org/10.4271/2017-01-0546.

[7] Breda S, D'Orrico F, Berni F, d'Adamo A, Fontanesi S, Irimescu A and Merola S S 2019 Experimental and numerical study on the adoption of split injection strategies to improve air-butanol mixture formation in a DISI optical engine Fuel 243 104–124. doi: 10.1016/j.fuel.2019.01.111

[8] Iaccarino S, Breda S, d'Adamo A, et al. 2017 Numerical simulation and flame analysis of combustion and knock in a DISI optically accessible research engine *SAE International Journal of Engines* **10**(2) 576-592. doi:10.4271/2017-01-0555

[9] Sparacino S, Berni F, d'Adamo A, Krastev V K, Cavicchi A and Postrioti L 2019 Impact of the Primary Break-Up Strategy on the Morphology of GDI Sprays in 3D-CFD Simulations of Multi-Hole Injectors *Energies* **12** 2890. doi: 10.3390/en12152890

[10] Berni F, Sparacino S, Riccardi M, Cavicchi A, Postrioti L, Borghi M and Fontanesi S 2022 A zonal secondary break-up model for 3D-CFD simulations of GDI sprays, *Fuel* **309**, 122064, doi: 10.1016/j.fuel.2021.122064

[11] Fontanesi S, Cicalese G, d'Adamo A and Pivetti G 2011 Validation of a CFD Methodology for the Analysis of Conjugate Heat Transfer in a High Performance SI Engine *SAE Technical Paper* 2011-24-0132. https://doi.org/10.4271/2011-24-0132.

[12] Krastev V K, d'Adamo A, Berni F and Fontanesi S 2019 Validation of a zonal hybrid URANS/LES turbulence modeling method for multi-cycle engine flow simulation *International Journal of Engine Research* **21** 632-648. https://doi.org/10.1177/1468087419851905

[13] d'Adamo A, Breda S and Cantore G 2015 Large-eddy simulation of cycle-resolved knock in a turbocharged SI engine *Energy Procedia* **82** 45-50. doi:10.1016/j.egypro.2015.11.881

[14] d'Adamo A, Breda S, Berni F and Fontanesi S 2018 Understanding the origin of cycle-to-cycle variation using large-eddy simulation: Similarities and differences between a homogeneous low-revving speed research engine and a production DI turbocharged engine *SAE*

International Journal of Engines **12**(1) 45–56. doi: 10.4271/03-12-01-0007
[15] Fontanesi S, Cicalese G, d'Adamo A and Cantore G 2013 A methodology to improve knock tendency prediction in high performance engines *Energy Procedia* **45** 769–78. https://dx.doi.org/10.1016/j.egypro.2014.01.082
[16] d'Adamo A, Breda S, Berni F and Fontanesi S 2019 The potential of statistical RANS to predict knock tendency: Comparison with LES and experiments on a spark-ignition engine *Applied Energy* **249** 126 – 142. https://doi.org/10.1016/j.apenergy.2019.04.093
[17] Del Pecchia M, Breda S, d'Adamo A, Fontanesi S, et al. 2018 Development of Chemistry-Based Laminar Flame Speed Correlation for Part-Load SI Conditions and Validation in a GDI Research Engine *SAE International Journal of Engines* **11**(6). https://doi.org/10.4271/2018-01-0174.
[18] Breda S, d'Adamo A, Fontanesi S, et al. 2016 CFD analysis of combustion and knock in an optically accessible GDI engine *SAE International Journal of Engines* **9**(1) 641-656. doi: 10.4271/2016-01-0601
[19] Del Pecchia M, Sparacino S, Breda S and Cantore G 2019 Validation of a sectional soot model based on a constant pressure tabulated chemistry approach for PM, PN and PSDF estimation in a GDI research engine *AIP Conference Proceedings* **2191**, 020064. doi: 10.1063/1.5138797
[20] Berni F, Mortellaro F, Pessina V, Paltrinieri S, Pulvirenti F, Rossi V, Borghi M and Fontanesi S 2023 Modeling of gaseous emissions and soot in 3D-CFD in-cylinder simulations of spark-ignition engines: A methodology to correlate numerical results and experimental data *International Journal of Engine Research* **24**(5) 2149 -74, doi: 10.1177/14680874221112564
[21] Pessina V, Berni F, Fontanesi S, Stagni A and Mehl M 2022 Laminar flame speed correlations of ammonia/hydrogen mixtures at high pressure and temperature for combustion modeling applications *International Journal of Hydrogen Energy*, **47**(61), pp. 25780-94, doi: 10.1016/j.ijhydene.2022.06.007
[22] Kee R J, Rupley F M and Miller J A 1990 *The Chemkin Thermodynamic Data Base*, United States. https://doi.org/10.2172/7073290
[23] Kee R J, Rupley F M, Miller J A, et al. 2000 *CHEMKIN Collection, Release 3.6*, Reaction Design, Inc., San Diego, CA.
[24] Magnussen B F *The Eddy Dissipation Concept, A Bridge Between Science and Technology* ECCOMAS Thematic Conference on Computational Combustion, June 21-24 2005, Lisbon, Portugal.
[25] Magnussen B F *On the structure of turbulence and generalized eddy dissipation concept for chemical reaction in turbulent flow* AIAA 1981-42, 19th Aerospace Sciences Meeting, January 1981. https://doi.org/10.2514/6.1981-42
[26] Sfriso S, Berni F, Fontanesi S, d'Adamo A et al., 2023 A 3D-CFD Numerical Approach for Combustion Simulations of Spark Ignition Engines Fuelled with Hydrogen: A Preliminary Analysis *SAE Technical Paper* 2023-01-0207. https://doi.org/10.4271/2023-01-0207.
[27] Verhelst S, T'Joen C, Vancoillie J and Demuynck J 2010 A correlation for the laminar burning velocity for use in hydrogen spark ignition engine simulation *International Journal of Hydrogen Energy* **36** 957-974, https://doi.org/10.1016/j.ijhydene.2010.10.020
[28] Masri A R, Dibble R W and Barlow R S 1996 The structure of turbulent non-premixed flames revealed by Raman-Rayleigh-LIF measurements *Prog. Energy Combust. Sci.* **22**(4) 307-362.
[29] Barlow R S *Proc. of the International Workshop on Measurement and Computation of Turbulent Non-Premixed Flames* Sandia National Laboratories Report, July 26-27 1996, Naples, Italy. https://doi.org/10.2172/541794
[30] Hassel E P *Proc. of the Second International Workshop on Measurement and Computation of Turbulent Non-Premixed Flames* Sandia National Laboratories Report, June 3-4 1997, Heppenheim, Germany.
[31] Meier W *Proc. of the Third International Workshop on Measurement and Computation of Turbulent Non-Premixed Flames* Sandia National Laboratories Report, Sections 1-2, July 30

-August 1 1998, Boulder, Colorado.
[32] Barlow R et al. *Proc. of the Fourth International Workshop on Measurement and Computation of Turbulent Non-Premixed Flames* Sandia National Laboratories Report, Section 1, June 27-29 1999, Darmstadt, Germany.
[33] Barlow R and Frank J *Piloted CH4/Air Flames C, D, E, and F – Release 2.1,* Sandia National Laboratories Report, June 15 2007.
[34] Piloted Jet Flame Archive: https://tnfworkshop.org/data-archives/pilotedjet/ch4-air/
[35] GRI 3.0 Chemical Mechanism: http://combustion.berkeley.edu/gri-mech/version30/text30.html
[36] Simple Jet Flame Archive: https://tnfworkshop.org/data-archives/simplejet/dlrflames/
[37] Conaire M O, Curran H J, Simmie J M, Pitz W J and Westbrook C K 2004 A Comprehensive Modeling Study of Hydrogen Oxidation *International Journal of Chemical Kinetics* **36**(11) 603-622.
[38] H3 Flame Data Archive: https://www.dlr.de/vt/desktopdefault.aspx/tabid-3067/4635_read-6718/
[39] Antonelli M and Martorano L 2012 Realization and Testing of a Low Pressure Hydrogen Direct Injection Engine Using Commercial Injectors SAE Technical Paper 2012-01-0652, https://doi.org/10.4271/2012-01-0652
[40] Antonelli M and Martorano L *Analisi numerica e sperimentale dei processi di iniezione e miscelamento in un piccolo motore ad iniezione diretta di idrogeno* 67th ATI National Congress, September 11-14 2012, Trieste, Italy.
[41] CRECK Modeling Chemical Mechanism: http://creckmodeling.chem.polimi.it/menu-kinetics/menu-kinetics-detailed-mechanisms/107-category-kinetic-mechanisms/401-mechanisms-1911-syngas
[42] Berni F, Fontanesi S, Cicalese G 2017 A modified thermal wall function for the estimation of gas-to-wall heat fluxes in CFD in-cylinder simulations of high performance spark-ignition engines *Applied Thermal Engineering* **115** 1045-62, https://doi.org/10.1016/j.applthermaleng.2017.01.055
[43] Berni F, Cicalese G, Sparacino S and Cantore G 2019 On the existence of universal wall functions in in-cylinder simulations using a low-Reynolds RANS turbulence model *AIP Conference Proceedings* **2191**, 020019, doi: 10.1063/1.5138752
[44] Berni F, Cicalese G, Borghi M and Fontanesi S 2021 Towards grid-independent 3D-CFD wall-function-based heat transfer models for complex industrial flows with focus on in-cylinder simulations *Applied Thermal Engineering* **190**, 116838, ISSN 1359-4311, https://doi.org/10.1016/j.applthermaleng.2021.116838